Available online at www.sciencedirect.com
ScienceDirect
Trans. Nonferrous Met. Soc. China 31(2021) 1587−1598
Transactions of Nonferrous Metals Society of China
www.tnmsc.cn

Refinement and strengthening mechanism of Mg−Zn−Cu−Zr−Ca alloy solidified under extremely high pressure

Xiao-ping LIN[1,2,3], Yang KUO[1], Lin WANG[1], Jie YE[1], Chong ZHANG[1], Li WANG[2], Kun-yu GUO[2]

1. School of Materials Science and Engineering, Northeastern University, Shenyang 110819, China;
2. School of Resources and Materials, Northeastern University at Qinhuangdao, Qinhuangdao 066004, China;
3. State Key Laboratory of Rolling and Automation, Northeastern University, Shenyang 110819, China

Received 3 June 2020; accepted 11 January 2021

Abstract: Mg−Zn−Cu−Zr−Ca samples were solidified under high pressures of 2–6 GPa. Scanning electron microscopy and electron backscatter diffraction were used to study the distribution of Ca in the microstructure and its effect on the solidification structure. The mechanical properties of the samples were investigated through compression tests. The results show that Ca is mostly dissolved in the matrix and the Mg_2Ca phase is formed under high pressure, but it is mainly segregated among dendrites under atmospheric pressure. The Mg_2Ca particles are effective heterogeneous nuclei of α-Mg crystals, which significantly increases the number of crystal nuclei and refines the solidification structure of the alloy, with the grain size reduced to 22 μm at 6 GPa. As no Ca segregating among the dendrites exists, more Zn is dissolved in the matrix. Consequently, the intergranular second phase changes from MgZn with a higher Zn/Mg ratio to Mg_7Zn_3 with a lower Zn/Mg ratio. The volume fraction of the intergranular second phase also increases to 22%. Owing to the combined strengthening of grain refinement, solid solution, and dispersion, the compression strength of the Mg–Zn–Cu–Zr–Ca alloy solidified under 6 GPa is up to 520 MPa.

Key words: high pressure solidification; Mg−Zn−Cu−Zr−Ca alloy; Mg_2Ca particle; solution strengthening; grain refinement strengthening

1 Introduction

As lightweight structural metallic materials, magnesium alloys are widely used in industry. Owing to the low strength and poor plasticity of cast magnesium alloys [1], strengthening and toughening of magnesium alloys is a prevalent research topic. Recently, the dual-phase nano-crystalline Mg thin film has increased the strength of the magnesium alloy to 3.3 GPa [2]; their study highlighted a new approach demonstrating that the properties of Mg alloys can be improved using the strengthening mechanisms of fine grains, solutions, and dispersions.

High-pressure solidification is a type of solidification technology that plays an important role in material preparation [3−5]. According to the high-pressure solidification theory [6,7], the pressure always reduces the nucleation activation energy and increases the nucleation rate. In addition, pressure can inhibit atomic diffusion and increase the atomic diffusion activation energy.

Using high-pressure solidification, researchers have obtained microstructures with fine grains in binary alloys, such as Al, Mg, Zn and Ti [6−12]. They also found that high-pressure solidification increases the solubility of solute atoms in the matrix. LIU et al [13] and ZHU et al [14] studied the solidification structure of hypoeutectic Al−9.2%Si and hypereutectic Al−26.6%Si alloys subjected to a pressure up to 5.5 GPa. They found that the micro-

Corresponding author: Xiao-ping LIN, Tel: +86-13780356091, E-mail: 750798921@qq.com
DOI: 10.1016/S1003-6326(21)65600-5

structure of the hypoeutectic Al−9.2%Si alloy was composed of an ultra-high supersaturated solid solution, almost a single α(Al) phase. GUO [15] studied the solidification structure and mechanical properties of an Al–32%Mg alloy solidified under a pressure of 3 GPa. Their results showed that the solid solubility of Mg in the α(Al) matrix was up to 30 wt.% and the tensile strength of the alloy was 430 MPa, eight times that of the alloy solidified under normal pressure.

Recently, DU et al [16] studied the structure and mechanical properties of the Mg−6Zn−0.5Cu−0.2Zr alloy solidified under a high pressure of 6 GPa. Compared with the structure of this alloy solidified under normal pressure, the secondary dendrite arm spacing decreased from 35 to 10 μm, the solid solubility of Zn in the α-Mg matrix increased from 2.28% to 4.12%, and the intercrystalline second phases changed from a net-like lamellar eutectic to a slender strip or island-like structure. Consequently, the compressive strength of the alloy increased from 170 to 430 MPa. The improved compressive strength can be attributed to a combination of three factors: solid solution strengthening caused by the increased solubility of Zn in the matrix, dispersion strengthening resulting from the change of the second phase, and grain refinement strengthening. However, the results demonstrate that the strength improvement is limited because of the low refinement degree of the dendrite structure.

Inoculation can effectively refine the solidification structure by adding a grain refiner. Currently, Ca is believed to be an excellent grain refiner for magnesium alloys. The solubility of Ca in magnesium is relatively low (maximum solid solution of 0.82 wt.% at 517 °C), and most of Ca elements segregate near grain boundaries or form Mg_2Ca with a high melting point (715 °C) [17−19]. Based on our previous study, Ca was added to the Mg–Zn–Cu alloy to study its distribution and effect on the solidification structure of the alloy during high-pressure solidification. The mechanism for improving the mechanical properties of the alloy was further explored. And new preparation techniques to strengthen Mg alloys using the combined strengthening mechanisms of grain refinement, solid solution, and dispersion were developed.

2 Experimental

Mg−Zn−Cu−Zr−(Ca) ingots were prepared from pure magnesium (purity of 99.99%), pure zinc (purity of 99.99%), Cu−Zn (molar ratio of 7:3), Mg−30wt.%Zr, and Mg−30wt.%Ca master alloys using 2RRL−M8 vacuum melting equipment. The melting and pouring temperatures were 760 and 730 °C, respectively. Molten liquid was poured into a metal mold preheated to 500 °C, producing ingots with diameters of 30 mm. The chemical compositions of the alloy without Ca were 6.22% Zn, 0.52% Cu, 0.16% Zr, and balance Mg, and those of the alloy with Ca were 6.25% Zn, 0.49% Cu, 0.16% Zr, 0.96% Ca, and balance Mg, as measured using the ICAP6300 plasma spectrometry. The alloy ingots were homogenized for 48 h at 300 °C in a vacuum furnace and then cut into rods with 6 mm in diameter and 10 mm in length by using the spark cutting technique.

High-pressure solidification experiments were carried out using a CS−1V hexahedral hydraulic ram, as shown in Fig. 1. The cubic cavity was extruded in three directions using six hammers. The solidification pressures were set to be 2, 4 and 6 GPa.

Fig. 1 Schematic diagram of working principle of CS−1B type cubic hinge press

According to Clausius−Clapeyron equation, the melting temperature of Mg increases with increasing solidification pressure [11]. Therefore, the melting temperature under different pressures should be set [17−21].

To determine the melting temperatures of the Mg−Zn−Cu−Zr−(Ca) alloy under different pressures, the samples were heated for 15 min

under different pressures and then cooled to room temperature at a rate of 200 K/s under holding pressure. The liquidus temperature was determined according to the change in the solidification structure. Figure 2 shows the solidification microstructure of the samples heated under a pressure of 4 GPa. When the heating temperature was 800 °C, the grain shape of the solidified microstructure was hexagonal, with wider grain boundaries (Fig. 2(a)). When the heating temperature was 820 °C, "snowflake" structure appeared on the edge, and a clear dividing line was observed, indicating that melting began at this time (Fig. 2(b)). When the heating temperature was 840 °C, the microstructure of the alloy appeared as small snowflakes, indicating that the alloy had completely melted (Fig. 2(c)). Therefore, the heating temperature of the alloy under 4 GPa pressure was set to be 860 °C. Subsequently, the heating temperatures of the alloys under 2, 5, and 6 GPa were 830, 910, and 960 °C, respectively.

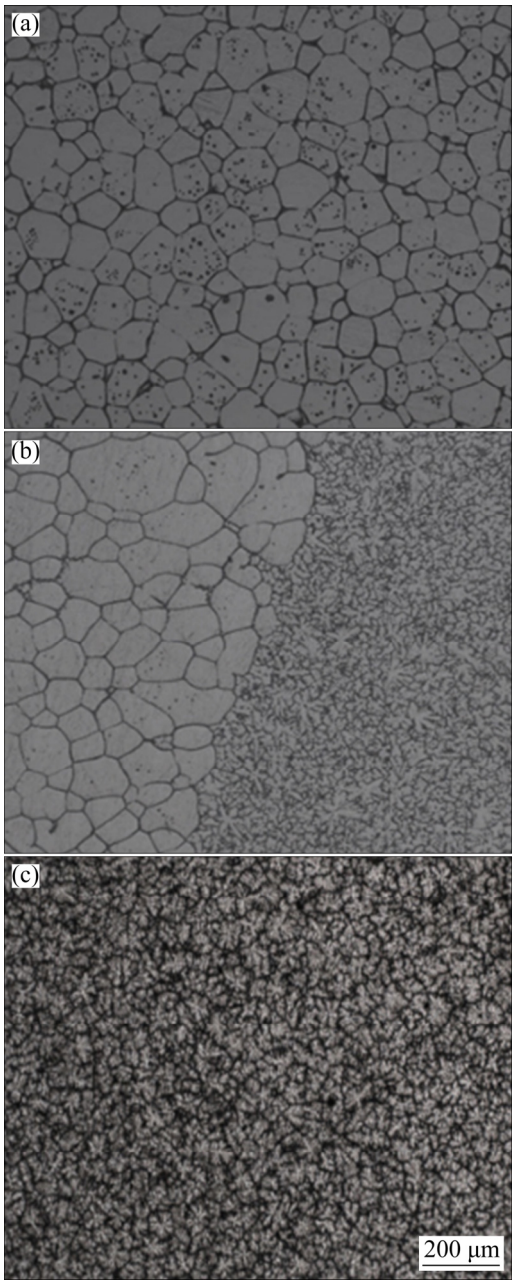

Fig. 2 Effect of heating temperature on OM microstructure under 4 GPa: (a) 800 °C; (b) 820 °C; (c) 840 °C

The sample was placed in the graphite sleeve [21], and then it was placed into the cavity of the hexahedral hydraulic ram. The hammers were placed toward the sample. The pressure was increased to the preset value, and the sample was rapidly heated to the preset temperature. After maintaining the temperature and pressure for 15 min, the power supply was turned off. Finally, the alloy samples were cooled to room temperature under holding pressure.

The microstructure of the alloy samples was observed using an i Scope A1 Pol optical microscope (OM) and a LEO JSM 5400 scanning electron microscope (SEM). The chemical composition of the samples was analyzed using SEM−EDS. Phase analysis was performed using a 2500/PC X-ray diffraction (XRD); the angle range (2θ) was 20°−80°, and the scanning step was 0.3°. The electron backscatter diffraction (EBSD) technique was used to analyze the grain size of the samples and the number of crystal and heterogeneous nuclei within the scanned area. EBSD specimens were cut, mechanically ground on 800−5000$^{\#}$ sandpapers, and subsequently electrolytically polished in a solution of 30% nitric acid alcohol. The EDAX TSL (Mahwah, NJ) OIM EBSD system was used, with Channel 5 for data analysis.

Compression tests were performed using a WWD3100 testing machine at a strain rate of 0.001 s^{-1} at room temperature. The hardness of the samples was tested using an HV−1000A tester with a load of 49 N. Testing 6−8 points on each sample resulted in the average hardness value.

3 Results and analysis

3.1 Solidification microstructure of Mg−Zn−Cu−Ca alloy

Figure 3 shows the microstructure of the cast Mg−Zn−Cu−Zr−(Ca) alloy solidified under atmospheric pressure. In Fig. 3(a), coarse dendrites

are observed, and some dendrites are fragmented. EBSD data showed that the average dendrite size is 262 μm, and the number of crystal nuclei in Fig. 3(a) is approximately 32.

Figure 4 shows the microstructure of Mg−Zn−Cu−Zr−(Ca) samples solidified under different pressures. Compared with Fig. 3(b), the primary dendrite α-Mg has fine and equiaxial "dendritic cluster" shape and the morphology of "dendrite cluster" is regular and complete, with few fragments and branches.

For the samples solidified under 2 and 4 GPa, the number of nucleus per unit area, the average size of the "dendrite cluster," and the secondary dendrite spacing were 108 and 203, 48 μm and 36 μm, and 14 μm and 11 μm, respectively. For the samples solidified under 6 GPa, the number of crystal nucleus per unit area increases to 252 (Fig. 5(a)), 7.9 times that of the sample solidified under atmospheric pressure. Meanwhile, the average size of the "dendrite cluster" and the secondary dendrite spacing are 24 μm and 6 μm, respectively.

Additionally, Figs. 4(c, d) and 5 show that the number of crystal nuclei of the Mg−Zn−Cu−Zr−Ca samples increases by 2.17 times and their secondary

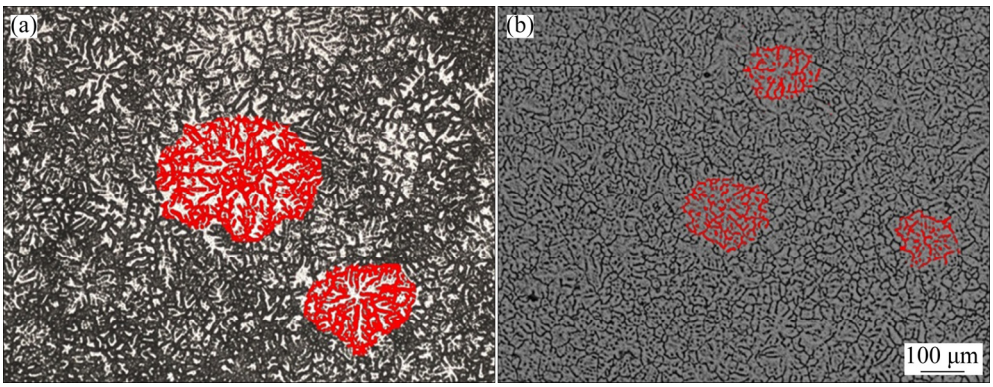

Fig. 3 Optical microstructures of alloy at atmospheric pressure: (a) Mg−Zn−Cu−Zr alloy; (b) Mg−Zn−Cu−Zr−Ca alloy

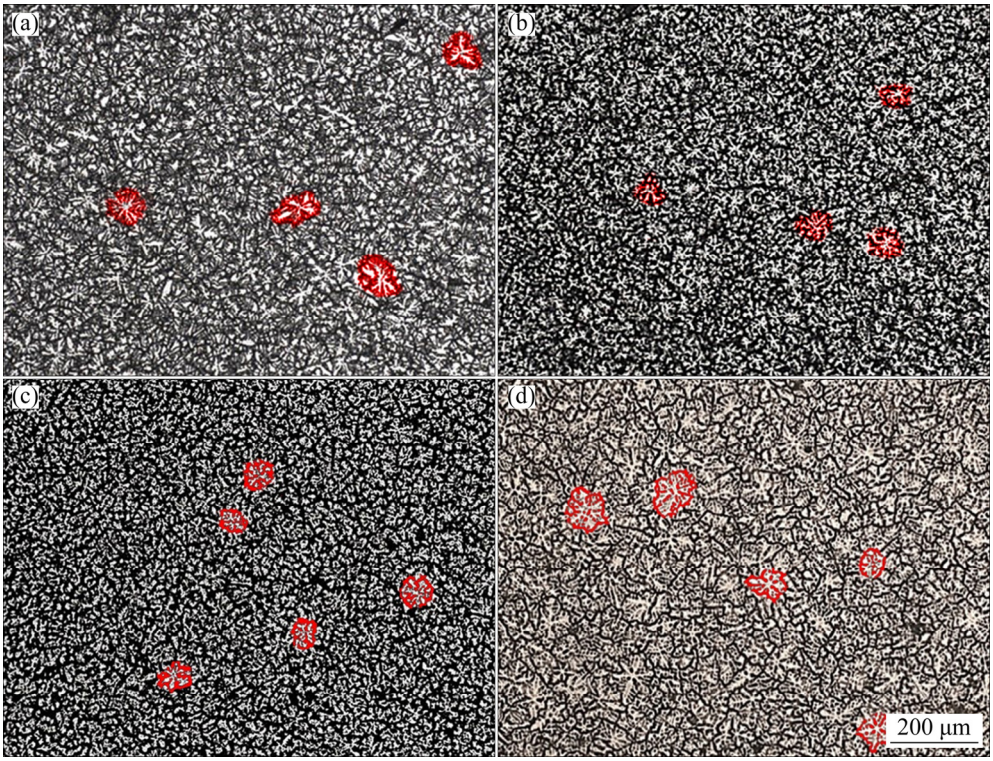

Fig. 4 Optical microstructures of Mg−Zn−Cu−Zr−(Ca) alloy solidified under different pressures: (a) Mg–Zn–Cu–Zr–Ca alloy, 2 GPa; (b) Mg–Zn–Cu–Zr–Ca alloy, 4 GPa; (c) Mg–Zn–Cu–Zr–Ca alloy, 6 GPa; (d) Mg–Zn–Cu–Zr alloy, 6 GPa

dendrite spacing decreases by 40% due to the addition of Ca under 6 GPa, compared with that of the Mg−Zn−Cu−Zr alloy (number of crystal nuclei per unit area is 116, and average dendrite size is 10 μm).

Figure 6 shows the effect of pressure and Ca addition on the grain size and the number of crystal nuclei of Mg−Zn−Cu−Zr alloy from EBSD data.

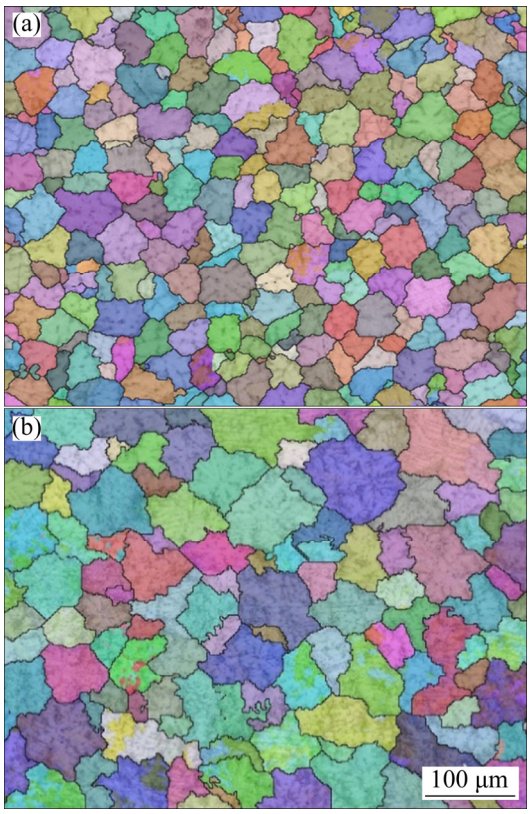

Fig. 5 EBSD orientation images of solidification structure of experimental alloy under 6 GPa: (a) Mg–Zn–Cu–Zr–Ca alloy; (b) Mg–Zn–Cu–Zr alloy

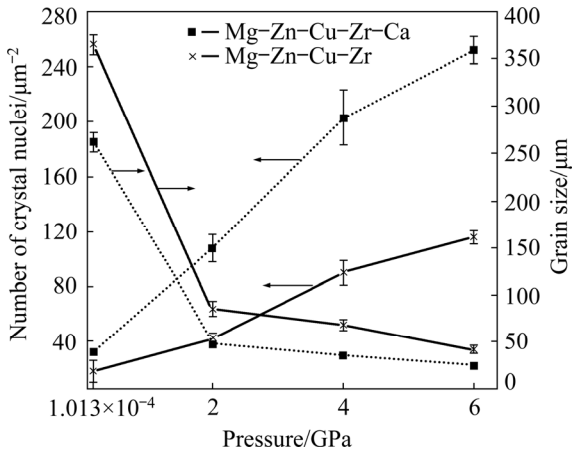

Fig. 6 Effect of solidification pressure and Ca addition on number and size of crystal nucleus of Mg–Zn–Cu–Zr alloy

The number of crystal nuclei increases and the grain size decreases with increasing the pressure, as demonstrated in Fig. 6. The addition of Ca can further increase the number of crystal nuclei and refine the solidification structure of the alloy under high pressure.

Figure 7 shows the effect of different pressures on the solidified microstructure of the Mg−Zn−Cu−Zr−Ca alloy. The second phase within the solidification structure of the alloy is mostly reticulate and distributed among the α-Mg dendrite, characterizing symbiotic eutectic structure (Figs. 7(a, b)). Under 2 GPa, the morphology and distribution of the second phase are similar to those of the alloy under normal pressure (Figs. 7(c, d)). With increasing pressure, the reticulate second phase among dendrites is not broken. However, the second phase gradually changes from the symbiotic eutectic to the divorced eutectic ("solid island-like"), and the amount of the granular or broken island-like second phase significantly increases (Figs. 7(e, h)). In addition, compared with the Mg−6Zn−0.5Cu−0.16Zr alloy solidified under high pressure, the volume fraction of the intergranular second phase increases significantly with the addition of Ca, which is twice that of the Mg−Zn−Cu−Zr alloy at 6 GPa, about 22%.

Figure 8 shows the distribution of Zn, Cu and Ca in Mg−Zn−Cu−Zr−Ca alloy solidified under different pressures. Under atmospheric pressure, Zn, Cu and Ca elements tend to be segregated among the α-Mg dendrites and their amounts are relatively less in the matrix (Figs. 8(a, c, e)). In addition, the EDS data show that the solid solubility of Zn in the α-Mg matrix is 3.36 wt.% and that of Ca is only 0.07 wt.% (Table 1). Under 6 GPa, the segregation degree of Zn among dendrites is greatly reduced, more Zn element is dissolved into the α-Mg matrix, and the distribution of Zn in the grains is more uniform, as shown in Fig. 8(b). From the EDS data, the solid solubility of Zn in the α-Mg matrix is 5.54 wt.% under 6 GPa. For the Mg−Zn−Cu−Zr alloy solidified under 6 GPa, the solid solubility of Zn in the matrix is 4.12 wt.%. The addition of Ca further increases the solid solubility of Zn in the α-Mg matrix. It should be noted that Ca is distributed homogeneously in the matrix under 6 GPa, except for a few "Ca particle", as shown in Fig. 8(f).

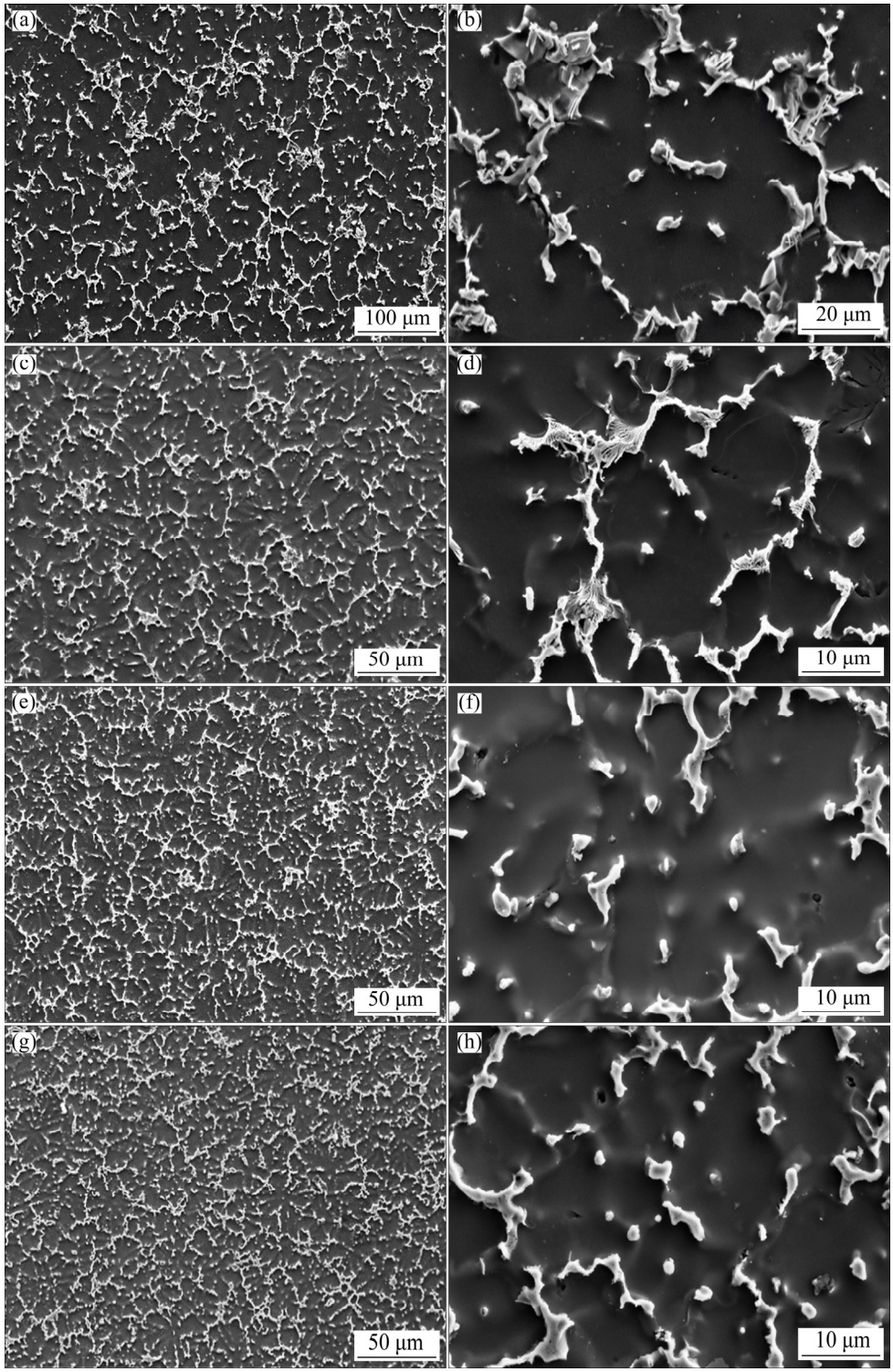

Fig. 7 Effect of solidification pressure on morphology of second phase in microstructure of Mg−Zn−Cu−Zr−Ca alloy: (a, b) Atmospheric pressure; (c, d) 2 GPa; (e, f) 4 GPa; (g, h) 6 GPa

Figure 9 shows the XRD patterns of Mg−Zn−Cu−Zr−Ca samples solidified under different pressures. The microstructure of the Mg−Zn−Cu−Zr−Ca alloy solidified under atmospheric pressure is mainly composed of α-Mg, $MgZn_2$, CuMgZn and Mg_2Ca phases, according to the XRD and EDS data. At 2 GPa, the characteristic diffraction peaks of CuMgZn phase (2θ=21.4°, 43.2° and 67.4°) are observed. At 6 GPa, the CuMgZn phase is hardly observed, but the characteristic diffraction peaks of Mg_7Zn_3 (2θ=23.7°, 36.7°, 38.9° and 39.6°) are observed. The characteristic diffraction peaks of

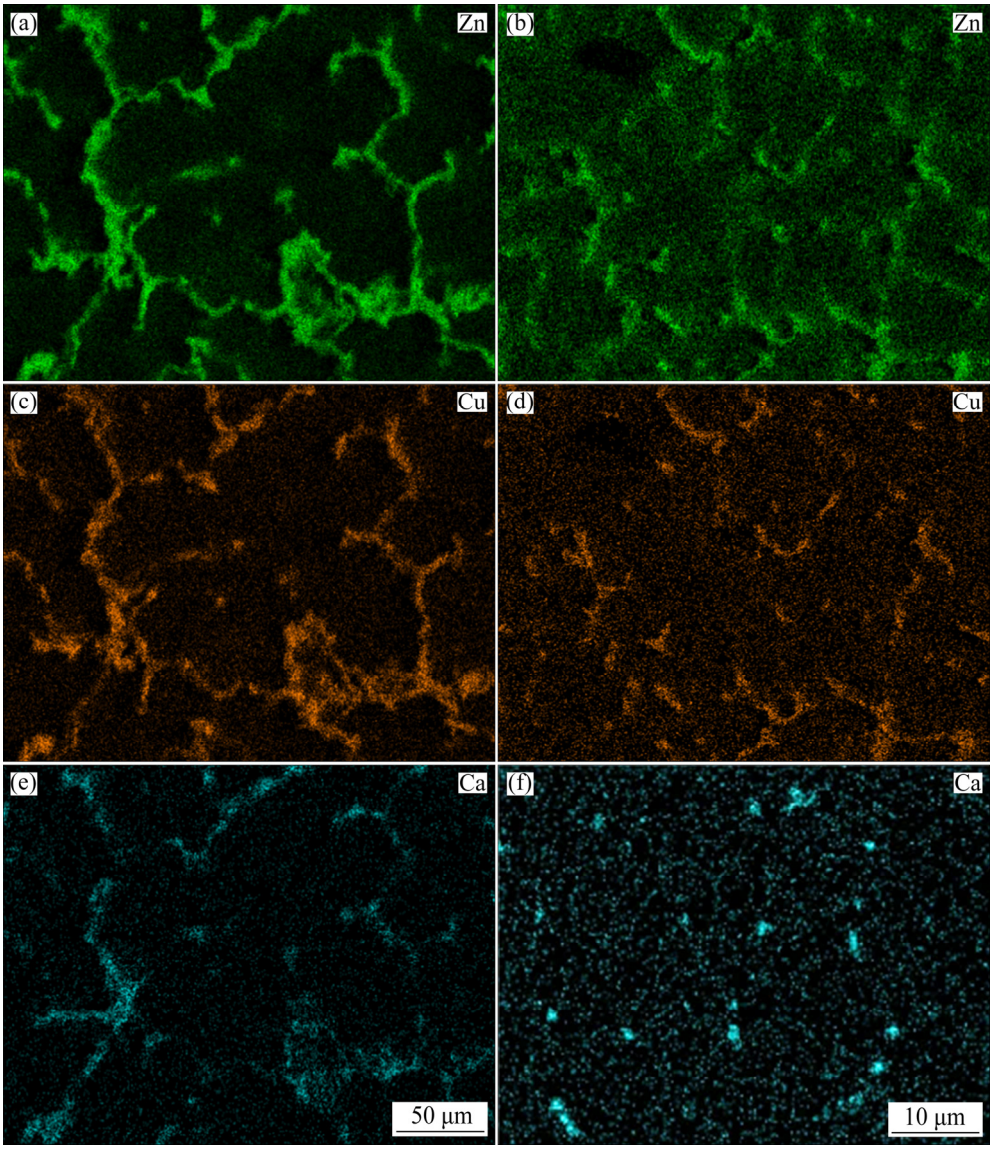

Fig. 8 SEM images of Mg−Zn−Cu−Zr−Ca alloy: (a, c, e) Conventional cast alloy; (b, d, f) Alloy solidified under 6 GPa

Table 1 Characteristic values of solidification microstructure and mechanical properties of Mg−Zn−Cu−Zr−Ca alloy

Pressure/GPa	Solidification microstructure characteristics			Solubility/wt.%			Mechanical properties	
	Number of crystal nuclei/μm^{-2}	Size of "dendritic cluster"/μm	Secondary dendrites spacing/μm	Zn	Cu	Ca	Hardness (HV)	Maximum breaking resistance, σ_b/MPa
1.013×10^{-4}	32	262	21	3.36	0.12	0.07	62	240
2	150	48	14	4.49	0.28	0.04	75	409
4	170	36	11	5.08	0.36	0.04	88	453
6	430	22	6	5.54	0.45	0.06	109	520

$MgZn_2$ (2θ=41.5°, 41.8°, 68.7°, 70.1° and 78.3°) are also found on the pattern of the alloy solidified under 6 GPa. Thus, the microstructure of the Mg−Zn−Cu−Zr−Ca alloy solidified under 6 GPa mainly consists of α-Mg, Mg_7Zn_3, $MgZn_2$ and Mg_2Ca.

The crystal structure of Mg and Zn is HCP, and that of Ca is FCC. The atomic radii of Mg, Zn, and Ca are 150, 138 and 180 pm, respectively. The atomic size difference between Zn and Mg is 8%, whereas it is 20% between Ca and Mg; therefore, the solid solubility of Ca in α-Mg is relatively low

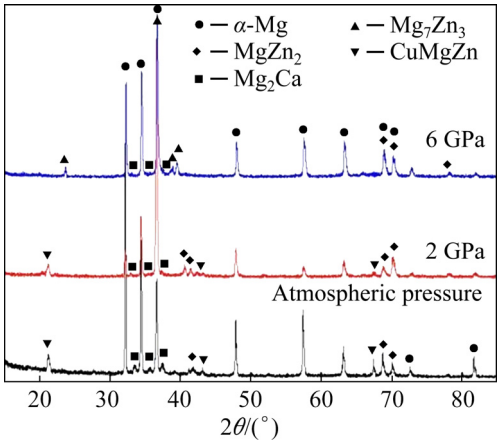

Fig. 9 XRD patterns of Mg−Zn−Cu−Zr−Ca alloy solidified under different pressures

under atmospheric pressure. Owing to the equilibrium partition coefficients, k_0<0, the concentration of solute atoms in the liquid phase at the solid–liquid interface continuously increases during solidification. As Ca is a surface-active element for Mg, Ca is adsorbed on the solid surface during the crystallization of α-Mg, which can reduce the surface energy of the solid–liquid interface and hinder the transfer of other solute elements (Zn, Cu, etc). Because of the slow diffusion of Ca, undercooling will occur near the liquid-phase interface; hence, the nucleation ratio of α-Mg increases. In summary, the above factors can inhibit the growth of α-Mg grains. For the alloy solidified under atmospheric pressure, Ca is mainly enriched among the α-Mg dendrites, and the solidification structure can be refined to a certain extent.

For the alloy solidified under extremely high pressure, the diffusion of solute atoms is difficult, and the redistribution of solute atoms is weakened during solidification, owing to exponential decay of the solute atom diffusion coefficient [22−29]. During the solidification process, the solid solubility of Zn in the α-Mg matrix gradually increases with increasing pressure, and the segregation degree of Zn among the α-Mg dendrites is lower than that under atmospheric pressure, resulting in a decrease in the atomic percentage of Zn in the intergranular second phase. Therefore, the diffraction peak intensity of the CuMgZn phase with a high Zn/Mg ratio is gradually weakened, whereas that of the Mg_7Zn_3 phase with a lower Zn/Mg ratio is gradually enhanced. Ca, with a larger difference in atomic radius, is more difficult to diffuse, and almost completely dissolves in the matrix without dendrite segregation. When the solidification pressure is high enough, Ca will be expelled from the matrix, forming many Mg_2Ca particles [14] that may become effective heterogeneous nuclei of α-Mg during high-pressure solidification.

The orientation relationships analyzed by EBSD are shown between the $MgZn_2$ particles and α-Mg matrix in Figs. 10(a, b), and between the Mg_2Ca particles and α-Mg matrix in Figs. 10(c, d).

The crystal structures of $MgZn_2$ and Mg are both HCP; the positions of $[1\bar{2}10]_{MgZn_2}$ Kikuchi pole and $[1\bar{2}10]_{\alpha\text{-Mg}}$ Kikuchi pole are very close, and the $(10\bar{1}0)_{MgZn_2}$ Kikuchi band is parallel to the $(10\bar{1}0)_{\alpha\text{-Mg}}$ Kikuchi band, as shown in Figs. 10(a, b). Therefore, the orientation relationship between the $MgZn_2$ and α-Mg matrix is $[1\bar{2}10]_{MgZn_2}$ // $[1\bar{2}10]_{\alpha\text{-Mg}}$ and $(10\bar{1}0)_{MgZn_2}$ //$(10\bar{1}0)_{\alpha\text{-Mg}}$. Similarly, from Figs. 10(c, d), the orientation relationship between Mg_2Ca and α-Mg matrix is $[0001]_{Mg_2Ca}$ // $[1\bar{2}10]_{\alpha\text{-Mg}}$ and $(0001)_{Mg_2Ca}$ //$[10\bar{1}0]_{\alpha\text{-Mg}}$.

According to the EBSD data, $MgZn_2$ and Mg_2Ca with the HCP structure become effective heterogeneous nuclei substrates of α-Mg during high-pressure solidification when Ca is added to the alloy. Most Ca elements are effective heterogeneous nuclei substrates of α-Mg in the form of tiny Mg_2Ca particles under extremely high pressure, increasing the number of crystal nuclei and refining the microstructure, which is different from the role of Ca under atmospheric pressure.

In summary, the number of crystal nuclei within the measured area increases from 116 to 252, and the size of the “dendrite cluster” decreases from 48 to 22 μm after Ca is added to the M−Zn−Cu−Zr alloy at 6 GPa. In addition, the solubility of Zn in the α-Mg matrix increases from 4.12% to 5.54%. As more Zn dissolves into the matrix, the intergranular second phase changes from the CuMgZn phase with a higher Zn/Mg ratio to the Mg_7Zn_3 phase with a lower Zn/Mg ratio, and most show discontinuous island or particle shape.

3.2 Mechanical properties of Mg−Zn−Cu−Zr−Ca alloy

Figure 11 displays the relationship between the hardness and solidification pressure of the alloys. With the addition of Ca, the hardness of the alloy

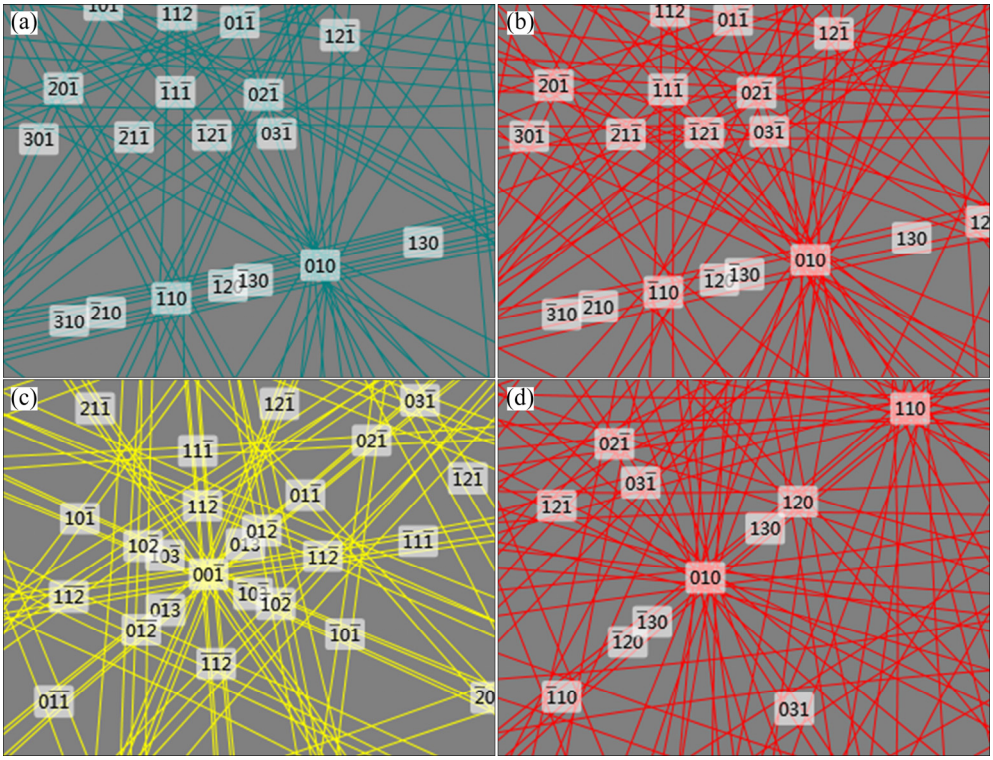

Fig. 10 EBSD patterns of particle phase in solidified Mg−Zn−Cu−Zr−Ca alloy and its surrounding Mg matrix under 6 GPa: (a, b) $MgZn_2$/α-Mg; (c, d) $MgCa_2$/α-Mg

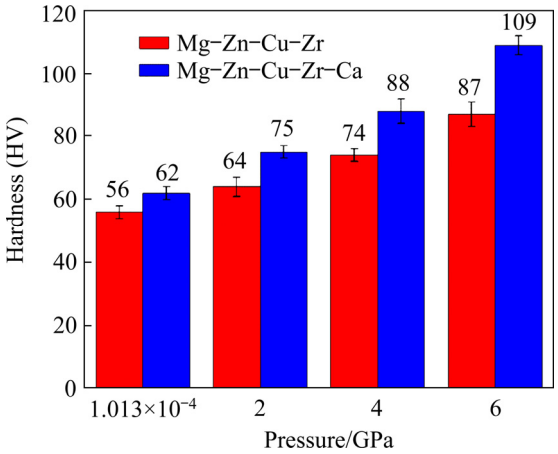

Fig. 11 Effect of solidification pressure on hardness of Mg−Zn−Cu−Zr−Ca alloy

increases under atmospheric pressure, owing to the refinement of grains and the amount increase of the second phase.

Thereafter, the hardness of the alloys increases with increasing pressure. At 4 and 6 GPa, the hardness values of the Mg−Zn−Cu−Zr−Ca alloy reach HV 88 and HV 109, respectively. Compared with the alloy without Ca, the Mg−Zn−Cu−Zr−Ca alloy has higher hardness. This is related to finer grains, higher solid solubility of Zn in the matrix, and more granular or island-like second phase.

Figures 12 and 13 show the compression properties of the alloys under different pressures. The compressive strength (σ_b) of the alloy with Ca addition increases from 170 to 228 MPa, and the relative compressibility (δ) increases from 11.2% to 14.8%. Further, σ_b of the alloy increases to 409 MPa, and δ also increases to 21% at 2 GPa. Thereafter, the strength of the alloy increases with increasing pressure, but the plasticity decreases. Under a pressure of 6 GPa, the σ_b value of the Mg−Zn−Cu−Zr−Ca alloy is up to 520 MPa. The strength has exceeded the highest strength value (380 MPa) of the cast Mg−Gd−Y−Zn alloy reported so far [17]. Moreover, the Mg−Zn−Cu−Zr−Ca alloy retains appropriate plasticity (16.6%). The improved mechanical properties can be attributed to the following factors: (1) strengthening caused by the refinement of the solidification structure with the addition of Ca, (2) solid solution strengthening resulting from further increases in the solubility of Zn in the matrix, and (3) dispersion strengthening caused by the increase of the granular or island-like second phase. Therefore, on account of the combination of grain refinement strengthening,

solid solution strengthening, and dispersion strengthening, the compression strength of Mg−Zn−Cu−Zr−Ca alloy solidified under 6 GPa is up to 520 MPa.

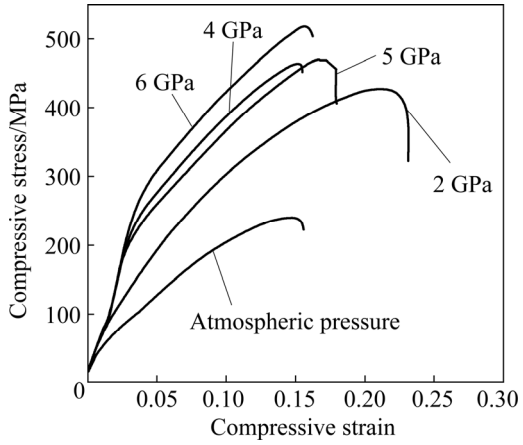

Fig. 12 Stress−strain curves of Mg−Zn−Cu−Zr−Ca alloy

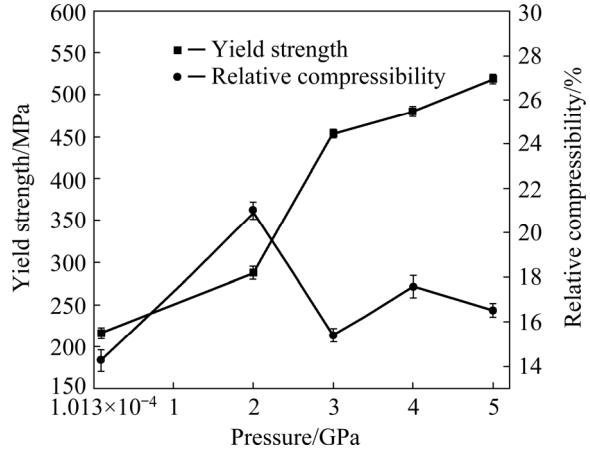

Fig. 13 Relationship of mechanical performance and solidification pressure

4 Conclusions

(1) During solidification under extremely high pressure, the pressure can increase the number of crystal nuclei by reducing the critical nucleation energy and critical nucleus radius of heterogeneous nucleation, as well as decreasing the interfacial tension. Simultaneously, owing to the addition of Ca, Mg_2Ca particles are gradually formed in the alloy with the increase in solidification pressure. Mg_2Ca and $MgZn_2$ become effective heterogeneous nuclei of α-Mg, which profoundly refines the microstructure. The grain size is reduced from 262 to 22 μm.

(2) Under high pressure, Ca element is mostly distributed in the matrix or forms Mg_2Ca particles, and more Zn is dissolved in the matrix. Therefore, the intergranular second phase gradually changes from the CuMgZn phase with a higher Zn/Mg ratio to the Mg_7Zn_3 phase with a lower Zn/Mg ratio, and the volume fraction of the intergranular second phase increases.

(3) Owing to the addition of Ca, the solidification structure of the alloy is further refined. Moreover, the solid solubility of Zn in the matrix increases, and the volume fraction of the intergranular second phase also increases. Therefore, the compression strength of the Mg−Zn−Cu−Zr−Ca alloy is as high as 520 MPa. Moreover, the Mg−Zn−Cu−Zr−Ca alloy retains appropriate plasticity (16.6%).

Acknowledgments

The authors appreciate the financial supports from the National Natural Science Foundation of China (Nos. 51675092, 51775099), and the Natural Science Foundation of Hebei Province, China (Nos. E2018501032, E2018501033).

References

[1] LI G Q, ZHANG J H, WU R Z, FENG Y, LIU S J, WANG X J, JIAO Y F, YANG Q, MENG J. Development of high mechanical properties and moderate thermal conductivity cast Mg alloy with multiple RE via heat treatment [J]. Materials Science & Technology, 2018, 34: 1076−1084.

[2] SWETHA S, RAVIKUMAR D, ANAND K, KONDAIAH V, RATNA S. Influence of heat treatment on the machinability and corrosion behavior of AZ91 Mg alloy [J]. Magnesium Alloy, 2018, 6: 52−58. doi:10.1016/j.jma.2017.12.001.

[3] DONG Q, LUO Z, ZHU H, WANG L Y, YING T, JIN Z H, LI D H, DING W J, ZENG X Q. Basal-plane stacking-fault energies of Mg alloys: A first-principles study of metallic alloying effects [J]. Materials Science & Technology, 2018, 34: 1773−1780. doi:10.1016/j.jmst.2018.02.009.

[4] HUANG L, LIU S H, DU Y, ZHANG C. Thermal conductivity of the Mg−Al−Zn alloys: Experimental measurement and CALPHAD modeling [J]. Calphad, 2018, 62: 99−108. doi:10.1016/j.calphad.2018.05.011.

[5] JIANG W, ZOU C M, HUANG H, RAN Z, WEI Z J. Crystal structure and mechanical properties of a new ternary phase in Mg−Zn−Y alloy solidified under high pressure [J]. Alloys and Compounds, 2017, 717: 214−218. doi:10.1016/j.jallcom.2017.05.088.

[6] ZHAO S S, PENG Q M, LI H, LIU B Z. Effects of super-high pressure on microstructures, nano-mechanical behaviors and corrosion properties of Mg−Al alloys [J]. Alloys and Compounds, 2014, 584: 56−62. doi:10.1016/j.jallcom.2013. 09.026.

[7] MA P, WEI Z J, JIA Y D, ZOU C M, SCUDINO S,

PRASHANTH K G, YU Z S, YANG S L, LI C G, ECKERT J. Effect of high pressure solidification on tensile properties and strengthening mechanisms of Al−20Si [J]. Alloys and Compounds, 2016, 688: 88−93. doi:10.1016/j.jallcom. 2016.07.016.

[8] FAN Z B, LIN X P, DONG Y, LI C, WANG L, FU S J. Dynamic recrystallization kinetic of fine grained Mg−Zn−Y−Zr alloy solidified under high pressure [J]. Journal of Rare Earths, 2017, 35: 920−926. doi:10.1016/ S1002-0721(17)60995-5.

[9] DONG Y, LIN X P, XU R, ZHENG R G, FAN Z B, LIU S J, WANG Z. Microstructure and compression deformation behavior in the quasicrystal-reinforced Mg−8Zn−1Y alloy solidified under super-high pressure [J]. Journal of Rare Earths, 2014, 32: 1048−1055. doi:10.1016/S1002-0721(14) 60182-4.

[10] ZHOU H T, LIU K M, ZHANG L, LU L, ATRENS A, LU D P. Influence of high pressure during solidification on the microstructure and strength of Mg−Zn−Y alloys [J]. Journal of Rare Earths, 2016, 34: 435−440. doi:10.1016/S1002-0721(16)60045-5.

[11] ZHANG W Q, XIAO W L, WANG F, MA C L. Development of heat resistant Mg−Zn−Al-based magnesium alloys by addition of La and Ca: Microstructure and tensile properties [J]. Alloys and Compounds, 2016, 684: 8−14. doi:10.1016/ j.jallcom.2016.05.137.

[12] CHEN X H, LIU L Z, PAN F S, MAO J J, XU X Y, YAN T. Microstructure, electromagnetic shielding effectiveness and mechanical properties of Mg−Zn−Cu−Zr alloys [J]. Materials Science & Engineering B, 2015, 197: 67−74. doi:10.1016/j.mseb.2015.03.012.

[13] LIU C, LIN X P, LI C, XU C, WANG T, LI Z. The influence of high pressure solidification process on solidification structure and properties of magnesium alloys [J]. Foundry, 2017, 66: 1057−1061. doi:10.3969/j.issn.1001-4977.2017. 10.005.

[14] ZHU H M, LUO C P, LIU J W, JIAO D L. Growth twinning behavior of cast Mg−Zn−Cu−Zr alloys [J]. Transactions of Nonferrous Metal Society of China, 2014, 24: 316−320. doi:10.1016/S1003-6326(14)63063-6.

[15] GUO Xue-feng. Preparation method, microstructure and properties of fine grain magnesium alloy [M]. Beijing: Metallurgical Industry Press, 2010. (in Chinese)

[16] DU Y Z, QIAO X G, ZHENG M Y, WU K, XU S W. The microstructure, texture and mechanical properties of extruded Mg−5.3Zn−0.2Ca−0.5Ce (wt%) alloy [J]. Materials Science & Engineering A, 2014, 620: 164−171. doi:10.1016/j.msea.2014.10.028.

[17] ZHANG J B, TONG L B, XU C, JIANG Z H, CHENG L R, KAMADO S, ZHANG H J. Influence of Ca−Ce/La synergistic alloying on the microstructure and mechanical properties of extruded Mg−Zn alloy [J]. Materials Science & Engineering A, 2017, 708: 11−20. doi:10.1016/j.msea. 2017.09.113.

[18] DONG Y, LIN X P, XU R, FAN Z B, YE J. Microstructure and room temperature compression properties of $Mg_{82.13}Zn_{13.85}Y_{4.02}$ alloy solidified under super-high pressure [J]. Acta Metallurgica Sinica, 2014, 50: 594−600. doi:10.3724/SP.J. 1037.2013.00504.

[19] MOTEGI T. Grain-refining mechanisms of superheat-treatment of and carbon addition to Mg−Al−Zn alloys [J]. Materials Science & Engineering A, 2005, 414: 408−411. doi:10.1016/j.msea.2005.08.214.

[20] FAN Z B, LIN X P, DONG Y, XU R, LI C, LIU N N. Constitutive model and deformation microstructure of fine-grain Mg−Zn−Y alloy solidified under high pressure [J]. Journal of Rare Earths, 2016, 34: 945−951. doi:10.1016/ S1002-0721(16)60119-9.

[21] WANG L, LIN X P, XU C, ZHAO S S, SUN H, ZHANG N. The microstructure and the mechanical property of AZ91D solidified under GPa-grade high-pressure [J]. Materials Science & Technology, 2019, 35: 1690−1699. doi:10.1080/ 02670836.2019.1639886.

[22] GB/T 6394 — 2002. Metal-methods for estimating the average grain size [S]. 2002.

[23] XU C, XU S W, ZHENG M Y, WU K, WANG E D, KAMADO S, WANG G J, LV X Y. Microstructures and mechanical properties of high-strength Mg−Gd−Y−Zn−Zr alloy sheets processed by severe hot rolling [J]. Alloys and Compounds, 2012, 524: 46−52. doi:10.1016/j.jallcom. 2012.02.050.

[24] SOMEKAWA H, SCHUH C A. Nanoindentation behavior and deformed microstructures in coarse-grained magnesium alloys [J]. Scripta Materialia, 2013, 68: 416−419. doi: 10.1016/j.scriptamat.2012.11.010.

[25] GHASSEMALI E, RIESTRA M, BOGDANOFF T, KUMAR B S, SEIFEDDINE S. Hall−Petch equation in a hypoeutectic Al−Si cast alloy: Grain size vs secondary dendrite arm spacing [J]. Procedia Engineering, 2017, 207: 19−24. doi:10.1016/j.proeng.2017.10.731.

[26] SUZUKI M, SATO H, MARUYAMA K, OIKAWA H. Creep deformation behavior and dislocation substructures of Mg−Y binary alloys [J]. Materials Science & Engineering A, 2001, 321: 751−755. doi:10.1016/s0921-5093(01)01005-x.

[27] DING Wen-jiang. Magnesium alloy science and technology [M]. Beijing: Science Press, 2007. (in Chinese)

[28] KLIMOVA M V, SHAYSULTANOV D G, ZHEREBTSOV S V, STEPANOV N D. Effect of second phase particles on mechanical properties and grain growth in a CoCrFeMnNi high entropy alloy [J]. Materials Science & Engineering A, 2019, 748: 228−235. doi:10.1016/j.msea.2019.01.112.

[29] JIE J C, ZHOU C M, WANG H W, WEI Z J. Mechanical behavior of Al−20Mg alloy solidified under high pressure [J]. Acta Metallurgica Sinica, 2014, 50: 971−978. doi:10.11900/ 0412.1961.2013.00767.

超高压下凝固 Mg−Zn−Cu−Zr−Ca 合金的组织细化与强化机制

林小娉[1,2,3]，阔 洋[1]，王 林[1]，叶 杰[1]，张 冲[1]，王 丽[2]，郭坤宇[2]

1. 东北大学 材料科学与工程学院，沈阳 110819；
2. 东北大学 秦皇岛分校 资源与材料学院，秦皇岛 066004；
3. 东北大学 轧制技术及连轧自动化国家重点实验室，沈阳 110819

摘 要：在 2~6 GPa 下对 Mg−Zn−Cu−Zr−Ca 合金进行凝固。利用 SEM 和 EBSD 等分析手段研究高压凝固过程中 Ca 的分布及对合金凝固组织的影响，并采用压缩试验研究合金的力学性能。结果表明，与常规铸造合金中 Ca 多偏聚在枝晶间不同，高压凝固合金中 Ca 多固溶于基体中以及形成 Mg_2Ca 质点相。Mg_2Ca 质点相为 α-Mg 晶体强有效的异质晶核，极大增加高压凝固过程总晶核数目并细化凝固组织，6 GPa 下合金晶粒尺寸细化至 22 μm。由于枝晶间无 Ca 偏聚，更多的 Zn 固溶到基体中，导致晶间第二相由 Zn/Mg 比较高的 MgZn 相(常压)逐渐转变为 Zn/Mg 比较低的 Mg_7Zn_3 相，并且晶间第二相体积分数增加至 22%。细晶强化、固溶强化以及弥散强化使 6 GPa 凝固的 Mg−Zn−Cu−Zr−Ca 合金强度高达 520 MPa。

关键词：高压凝固；Mg−Zn−Cu−Zr−Ca 合金；Mg_2Ca 质点相；固溶强化；细晶强化

(Edited by Bing YANG)